

N O T I C E

THIS DOCUMENT HAS BEEN REPRODUCED FROM
MICROFICHE. ALTHOUGH IT IS RECOGNIZED THAT
CERTAIN PORTIONS ARE ILLEGIBLE, IT IS BEING RELEASED
IN THE INTEREST OF MAKING AVAILABLE AS MUCH
INFORMATION AS POSSIBLE

9950-423

DOE/JPL-955640-81/7

DISTRIBUTION CATEGORY UC-63

(NASA-CR-163474) DEVELOPMENT AND
FABRICATION OF A SOLAR CELL JUNCTION
PROCESSING SYSTEM (Spire Corp., Bedford,
Mass.) 30 p HC A03/MF A01

N82-16490

CSCI 10A

Unclass

G3/44 08832

DEVELOPMENT AND FABRICATION OF A SOLAR CELL JUNCTION PROCESSING SYSTEM

QUARTERLY PROGRESS REPORT NO.7

OCTOBER 1981

THE JPL LOW-COST SOLAR ARRAY
PROJECT IS SPONSORED BY THE
U.S. DEPARTMENT OF ENERGY AND
FORMS PART OF THE SOLAR PHOTO-
VOLTAIC CONVERSION PROGRAM TO
INITIATE A MAJOR EFFORT TOWARD THE
DEVELOPMENT OF LOW-COST SOLAR
ARRAYS. THIS WORK WAS PERFORMED
FOR THE JET PROPULSION LABORATORY,
CALIFORNIA INSTITUTE OF TECHNOLOGY
BY AGREEMENT BETWEEN NASA AND DOE.



PREPARED UNDER CONTRACT NO. 955640 FOR:
JET PROPULSION LABORATORY
CALIFORNIA INSTITUTE OF TECHNOLOGY
PASADENA, CALIFORNIA 91103



DRD No. QR
CDRL Item No. 5


DOE/JPL-955640-81/7
Distribution Category UC-63

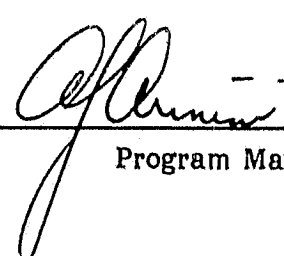
DEVELOPMENT AND FABRICATION OF A
SOLAR CELL JUNCTION PROCESSING SYSTEM

Report Number QR-10073-07
Quarterly Report No. 7

October 1981

This work was performed for the Jet Propulsion
Laboratory, California Institute of Technology,
sponsored by the National Aeronautics and Space
Administration under contract NAS7-100.

Prepared by: 
Project Engineer

Approved by: 
Program Manager

SPIRE CORPORATION
Patriots Park
Bedford, MA 01730

TABLE OF CONTENTS

<u>Section</u>		<u>Page</u>
1	CONTRACT OBJECTIVES	1
2	SUMMARY OF WORK PERFORMED.	4
3	PROGRESS ON TASK 1 - DEVELOPMENT OF THE PULSED ELECTRON BEAM SUBSYSTEM . .	5
	3.1 Pulser Fabrication	5
	3.2 Pulse Annealing Tests	5
	3.3 Non-mass Analyzed (NMA) Implantation	9
	3.3.1 Design Concept	12
	3.3.2 NMA Experimental Test Facility	12
	3.3.3 Solar Cell Data	20
4	SCHEDULE AND FUTURE WORK	25

LIST OF FIGURES

<u>Figures</u>		<u>Page</u>
1	Spire/JPL Junction Processor	2
2	Pulser and Transport	6
3	Cell Efficiency Versus Sheet Resistance - Low Values	10
4	Cell Efficiency Versus Sheet Resistance - High Values	11
5	NMA Ion Source Concept	13
6	High Throughput Ion Implantation System	14
7	NMA Test Implant Chamber	15
8	Test Model Beam Bender	17
9	Ions Produced by Commercial Grade Solid Phosphorus	18
10	Electrostatic Beam Bending at High Current	19
11	Ion Implanter Beam Spread After Bend/Defocus	21
12	Quantum Efficiency for NMA Implants and Center Controls	24
13	Task 3 - NMA Ion Implanter Fabrication	26

SECTION 1

CONTRACT OBJECTIVES

The basic objectives of the program are the following:

1. To design, develop, construct, and deliver a junction processing system which will be capable of producing solar cell junctions by means of ion implantation followed by pulsed electron beam annealing.
2. To include in the system a wafer transport mechanism capable of transferring 4-inch-diameter wafers into and out of the vacuum chamber where the ion implantation and pulsed electron beam annealing processes take place.
3. To integrate, test, and demonstrate the system prior to its delivery to JPL along with detailed operating and maintenance manuals.
4. To estimate component lifetimes and costs, as necessary for the contract, for the performance of comprehensive analyses in accordance with the Solar Array Manufacturing Industry Costing Standards (SAMICS).

In achieving these objectives, Spire will perform five tasks:

Task 1 - Pulsed Electron Beam Subsystem Development

Task 2 - Wafer Transport System Development

Task 3 - Ion Implanter Development

Task 4 - Junction Processing System Integration

Task 5 - Junction Processing System Cost Analyses

Under this contract the automated junction formation equipment to be developed involves a new system design incorporating a spire-designed ion implanter with a Spire-developed pulsed electron beam annealer and wafer transport system. Figure 1 presents a conceptual drawing of the junction processing system. When constructed, the ion implanter will deliver a 16 mA beam of $^{31}\text{P}^+$ ions with a fluence of 2.5×10^{15} ions per square centimeter at an energy of 10 keV. The throughput design goal rate for the junction processor is 10^7 four-inch-diameter wafers per year.

ORIGINAL PAGE IS
OF POOR QUALITY.

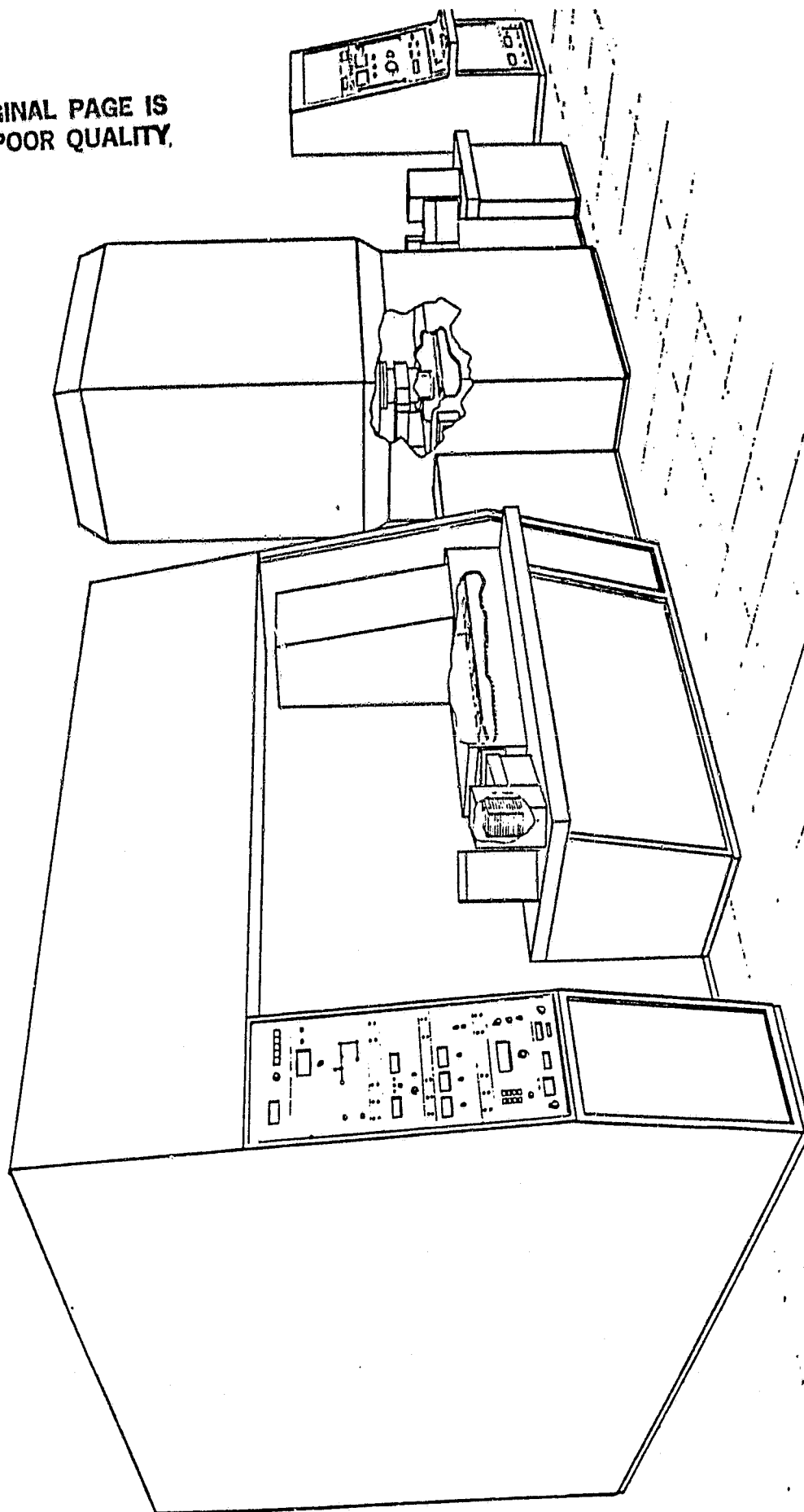


FIGURE 1. SPIRE/JPL JUNCTION PROCESSOR

At the present time, authorization has been given to perform work only on Tasks 1 through 3. The performance of Tasks 4 and 5 has been deferred until a written "Notice to Proceed" with one or more of these deferred tasks is received from JPL.

SECTION 2

SUMMARY OF WORK PERFORMED

This quarterly report covers work performed during the period between 1 July through 30 September 1981 on Tasks 1 to 3 of the contract for the development and fabrication of a solar cell junction processing system. Assembly and system testing has continued on the Task 1 phase to develop a pulsed electron beam for the 4-inch wafers. Wafers have been successfully pulsed and solar cells fabricated. Assembly of the transport locks has now been completed. The transport has been operated successfully but not yet with sufficient reproducibility. An experimental test facility to examine potential scaleup problems associated with the proposed ion implanter design has been constructed and operated. Cells have been implanted and found to have efficiency identical to the normal Spire implant process.

SECTION 3
PROGRESS ON TASK 1
DEVELOPMENT OF THE PULSED ELECTRON BEAM SUBSYSTEM

3.1 PULSER FABRICATION

The 300 kV power supply has arrived and enables the pulser to be operated in excess of 200 kV with greater stability than the previous 160 kV supply, which was at its upper limit. The new supply was found to operate smoothly with far fewer arc-over events, even though the geometry in the pulser was unchanged.

The high voltage cable has been replaced with a cable consistent with the voltage of the new supply. After about 500 shots, high voltage instability began to occur, and the problem was traced to a bad connection on a segment of the high voltage feed inside the pressure vessel. The connector was replaced and has not failed since. The rest of the unit was closely examined at this time for switch damage, capacitor damage, clustering of arc damage, or any other potential weaknesses in the high voltage design. None were observed.

The pulser unit is now considered complete with the exception that a high voltage monitor at the capacitor bank now appears to be required. With multiple shots in quick succession, there was sufficient thermal-induced change in the impedance of the charging resistor that a false drift was observed in the external monitoring circuit. This will be corrected by measuring the capacitor voltage directly with a voltage divider network. Parts for this circuit modification have been ordered.

The completed pulser and transport is shown are Figure 2.

3.2 PULSE ANNEALING TESTS

There exists an optimum geometry/voltage combination, which can produce a uniform electron beam with the required energy spectrum. Numerous tests were performed within the matrix of possible combinations of parameters to achieve a satisfactory balance.

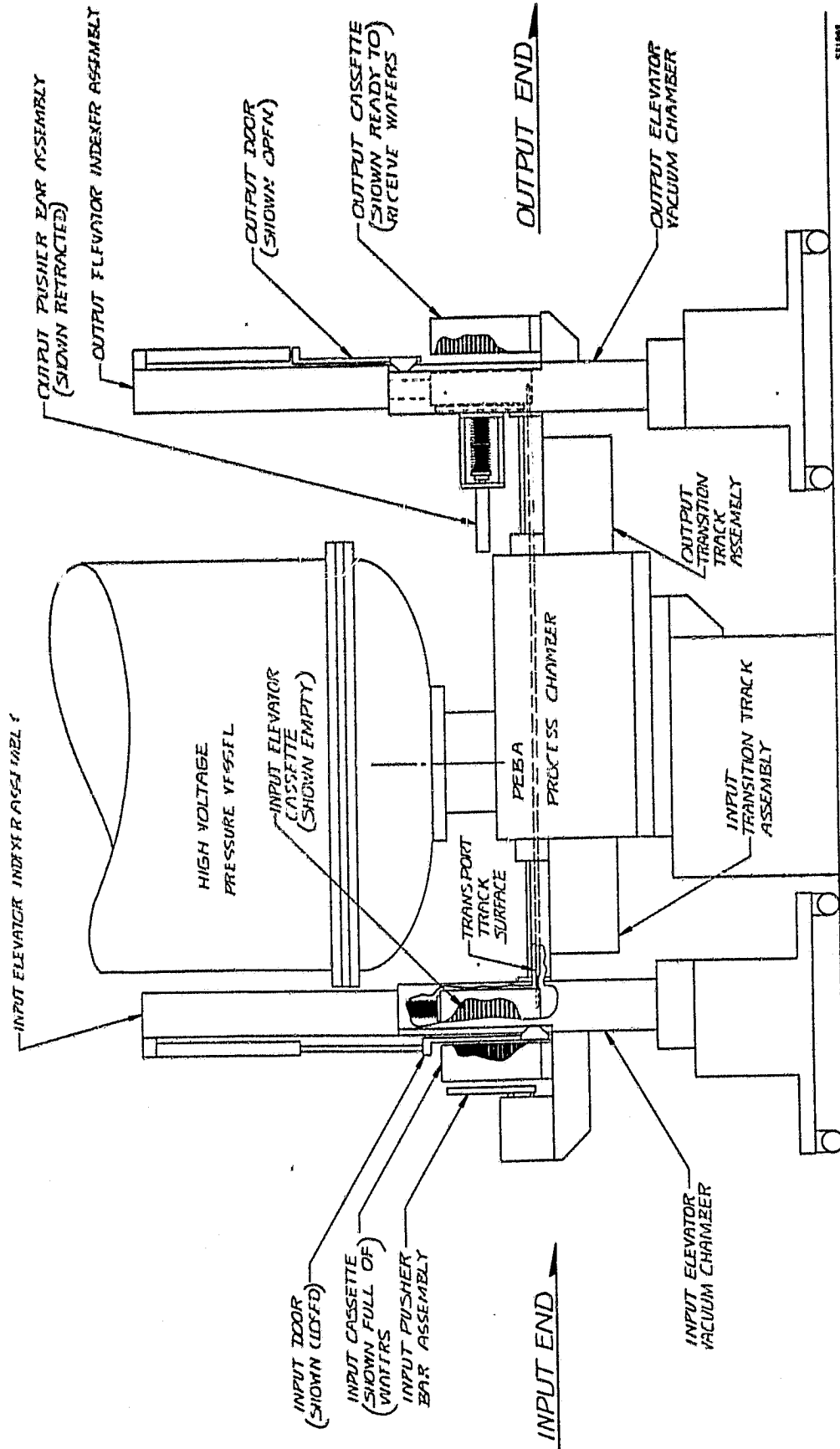


FIGURE 2. PULSER AND TRANSPORT

The best results obtained to date are for a 4.5-inch cathode. The anode-cathode gap was found to be 2.5 mm with a subsequent beam drift distance of 7.8 mm. The most uniform spot was at a charging voltage of 185 kV with an impressed axial magnetic field produced by 9 Amps through the coil.

The drift distance is nearly twice that reported in the last quarterly report. It has been found that beam uniformity and elimination of anode mesh shadowing required that the zone beyond the natural pinch of the electron beam be used.

The beam produced by this technique is sufficiently uniform to require visual examination of wafers to observe deficiencies that may be finer than the multi-point calorimeter is capable of detecting. A large number of wafers were implanted and pulsed to perform the final fine adjustments of geometrical parameters.

The best appearing wafers were made into solar cells at several stages in the electron beam studies. Table 1 lists the results of the best cells from wafers processed one month before the improved group shown in Table 2. In each case the "best" cells are shown. Although there has been little change in overall efficiency, the cells of Table 1 are individually good cells selected from 8 per wafer. There was poor uniformity of performance on each 4-inch wafer. In the more recent Table 2 lot, all of the cells that survived fabrication losses are shown for two wafers, demonstrating that a far more uniform anneal has now been created. However, some wafer-to-wafer variability remains, even though the performance tends to be uniform for all the cells made from a given wafer. This area of shot-to-shot repeatability will be the subject of further testing.

An experiment was performed to reproduce the thermal effects of an 850°C furnace treatment with a time history typical of an aluminum paste BSF. This test was performed on the early PEBA wafers only, before intra-wafer uniformity had been achieved. Table 3 shows the average results for the two cases. The results are inconclusive, mainly because of the large variability for the early trials. No major change in performance appears to be evident from these data.

TABLE 1. EARLY PEBA CELLS

Cell	V _{oc} (mV)	J _{sc} (mA/cm ²)	FF %	Eff (AM0) %
7-1	544	24.2	69.2	6.74
10-1	559	26.1	72	7.78
16-2	553	27.3	70.7	7.88
17-3	558	27.4	70.4	7.96
Control	563	28.1	76.2	8.90

No antireflection coating or back surface field

TABLE 2. JUNCTION PROCESSOR/PEBA CELLS

Lot Number:	4031	Resistivity:	10.0 ohm-cm
Surface:	Pol	AR Coating:	None
Comment:	PEBA	Material:	CZ
Cell Area:	4.0 cm ²	Thickness:	18 mils
Illumination:	AM0	Temperature:	25°C

Cell	V _{oc} (V)	J _{sc} (mA/cm ²)	FF %	Eff (AM0) %
71	0.540	29.4	71.9	8.45
72	0.540	29.3	69.8	8.15
73	0.535	29.0	71.6	8.20
74	0.540	29.1	68.9	8.01
75	0.540	29.1	69.3	8.05
76	0.543	29.1	72.8	8.50
91	0.545	28.5	71.9	8.25
94	0.553	28.2	73.8	8.50
Ave.	0.552	29.1	71.3	8.26
Sdv.	0.005	0.3	1.7	0.20

TABLE 3. CELL PERFORMANCE FOR PEBA PLUS SHORT ANNEAL

Wafer	Cells	V _{oc} (mV)	J _{sc} (mA/cm ²)	FF %	EFF %	Corr. AM1 Eff %
16	8	525	27.2	63.2	6.52	10.8
17	7	535	27.1	65.1	7.00	11.6
7	10	524	23.5	66.8	6.07	10.0
10	6	544	26.0	69.3	7.25	12.0
Control	19	564	28.1	71.7	8.52	14.1

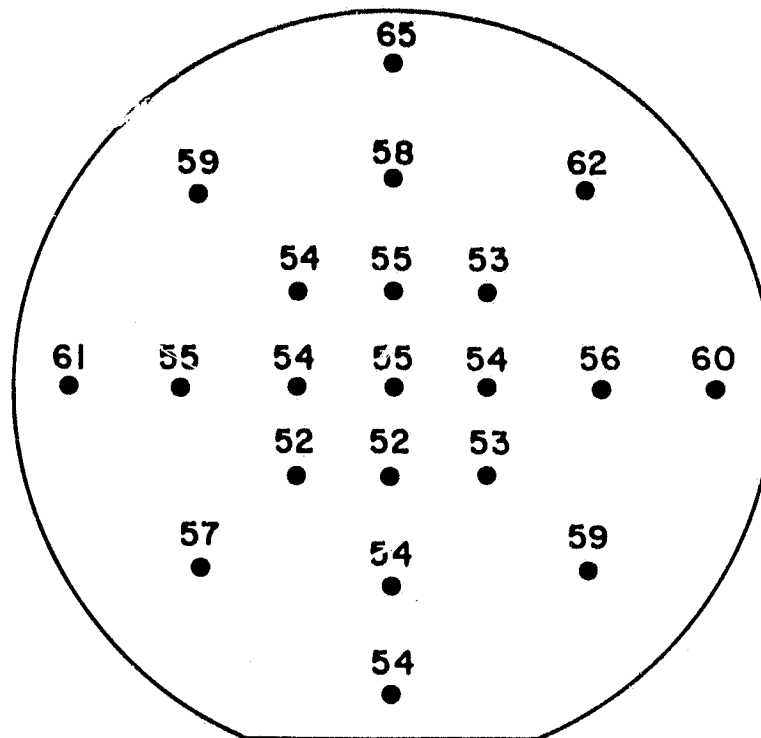
16, 17 PEBA
 7, 10 PEBA plus 850°C for 1 min
 Control Furnace Anneal

No antireflection coating or back surface field
 Corrected AM1 Eff. - Eff(AM0)x1.4x1.18

A test was made to correlate final cell performance with sheet resistance was performed. A wide range of sheet resistance for visually annealed 4-inch wafers was available. Figures 3 and 4 show cell performance for two of these wafers together with the location and efficiencies of 2x2 cm cells made from the 4-inch wafers. The higher sheet resistance appears to have marginally better performance. Microscopic surface examination of the cells of Figure 3 indicates the presence of damage zones not apparent to the eye which are not present on the cells of Figure 4. It is thus believed that some improvement in beam uniformity still remains to be accomplished.

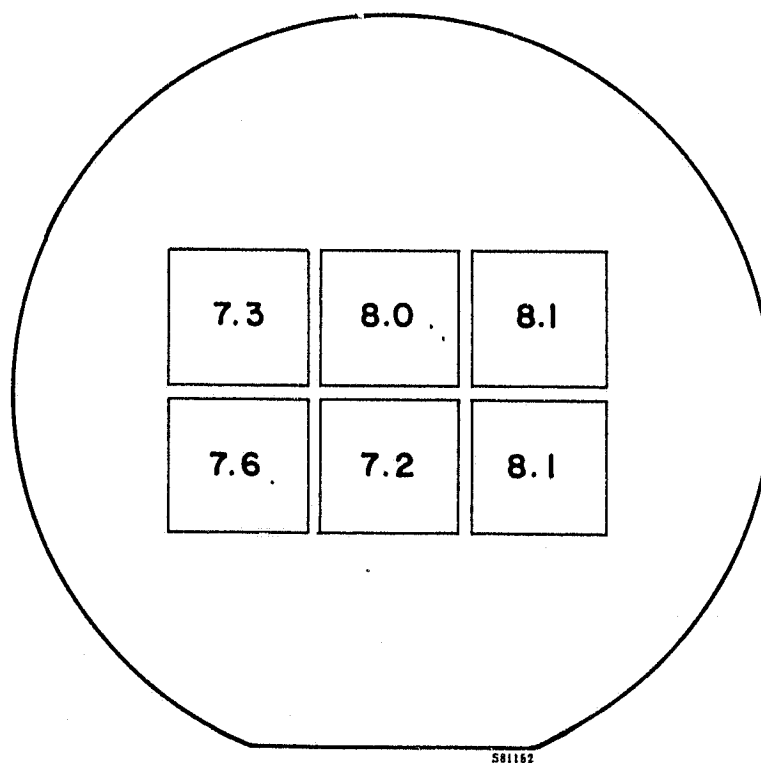
3.3 NON-MASS ANALYZED (NMA) IMPLANTATION

Task 3 is to design and construct a non-mass analyzed ion implanter, which is to be joined on Task 4 to the pulsed annealer to form the complete junction processor. The task was officially turned on in July and work has proceeded on design concepts and the fabrication of an experimental test facility.



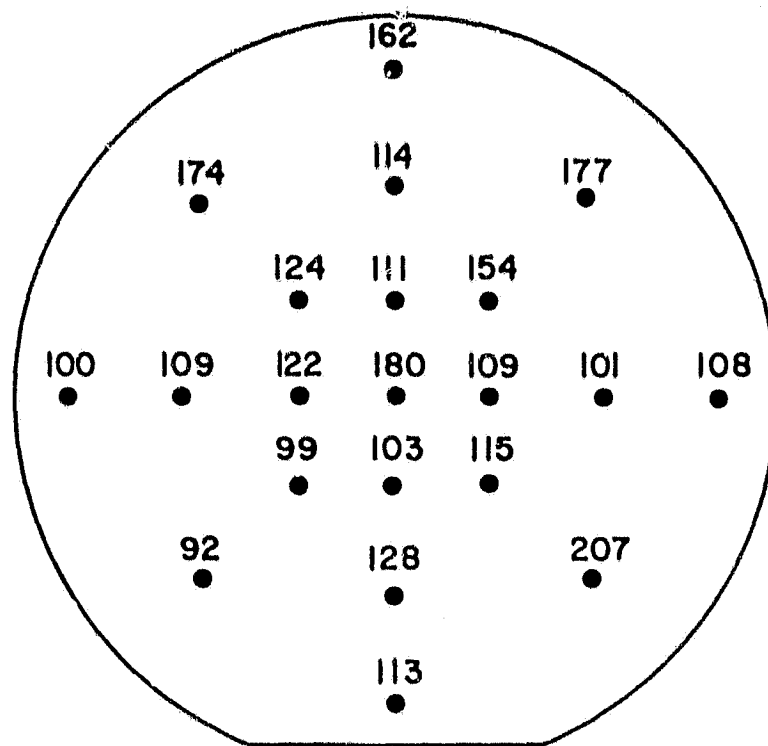
SHEET RESISTANCE
(Ω/\square)

WAFER No. 10



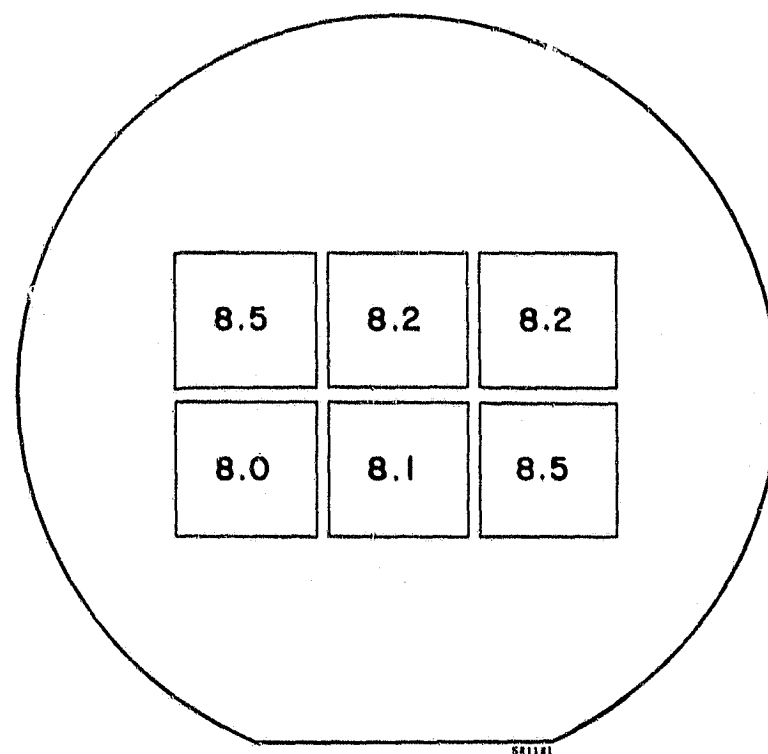
AMO EFF. (%)

FIGURE 3. CELL EFFICIENCY VERSUS SHEET RESISTANCE - LOW VALUES



SHEET RESISTANCE
(Ω/\square)

WAFER No. 7



AMO EFF. (%)

FIGURE 4. CELL EFFICIENCY VERSUS SHEET RESISTANCE - HIGH VALUES

3.3.1 Design Concept

Typical of the design concept work in progress is Figure 5, which shows the layout of components in the high current ion source. Figure 6 shows the complete setup, together with the end station locks on the transport. The present concept has only a 30° bend with a 10° angle of incidence on the wafer. This is based on results from the test facility which will be discussed presently.

The implantation system of Figure 6 shows a modified Freeman-type ion source, which is mounted with its own pumping system above the wafer transport. The primary modifications are for high current and extender lifetime of the phosphorus charge used in the boiler. An electrostatic bend is placed in the beam path to separate the residue neutral gas and to cause a defocus of the beam to match the area of the wafer. This defocus will largely be obtained from the natural space charge beam expansion which occurs in the electric field of the bender. The expansion is a result of the local loss in space charge neutralization due to the electric field of the bender sweeping the volume of low energy electrons.

The downstream zone above the wafer and track contains a Faraday cup arrangement with a removable Faraday flag. Monitors below the track are used for sampling the beam during wafer processing. Beam centering is performed by a combination of bender potential and geometry. Information feedback on centering will be available from below-track monitors and visually through appropriately placed ports on the vacuum chamber. The latter is possible because residual gas in the chamber glows with a characteristic wavelength when the ion beam impacts the atoms.

3.3.2 NMA Experimental Test Facility

It is very difficult to numerically predict certain aspects of the beam transport at the high currents intended for the NMA implants. Of special importance is the degree of defocusing provided by the space charge expansion in the bender. This will vary with the electric field used, beam current, beam shape, and geometry, but this dependence cannot be reliably predicted on the basis of theory. Therefore, it was decided to assemble a test setup based on commercial hardware that could serve to perform beam studies as well as implant a few wafers to a rough degree of uniformity. Figure 7 shows a diagram of the facility produced. The only components that had to be newly fabricated were the bender, the Faraday cup, the beam probe, and miscellaneous small parts.

ORIGINAL PAGE IS
OF POOR QUALITY

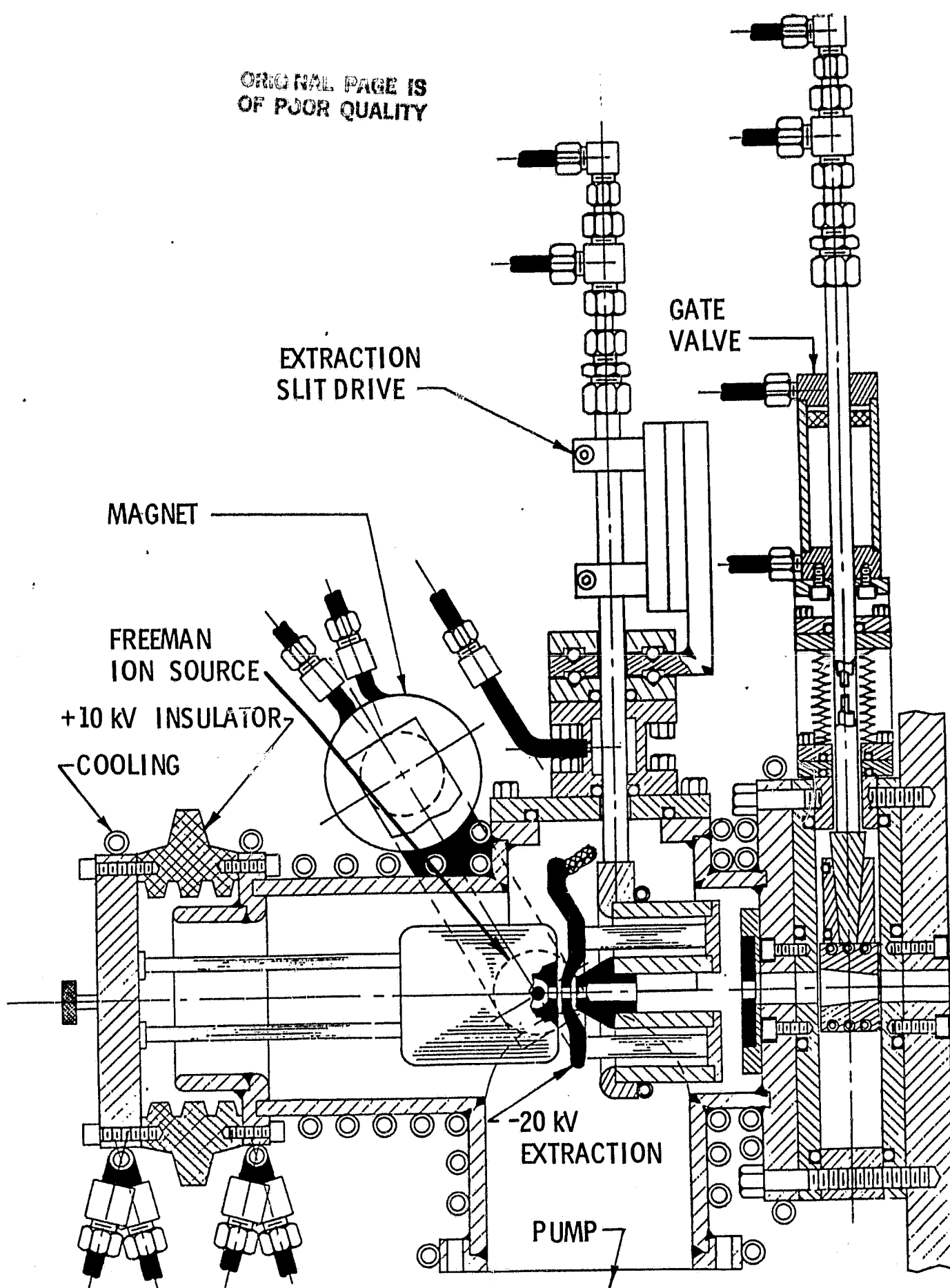


FIGURE 5. NMA ION SOURCE CONCEPT

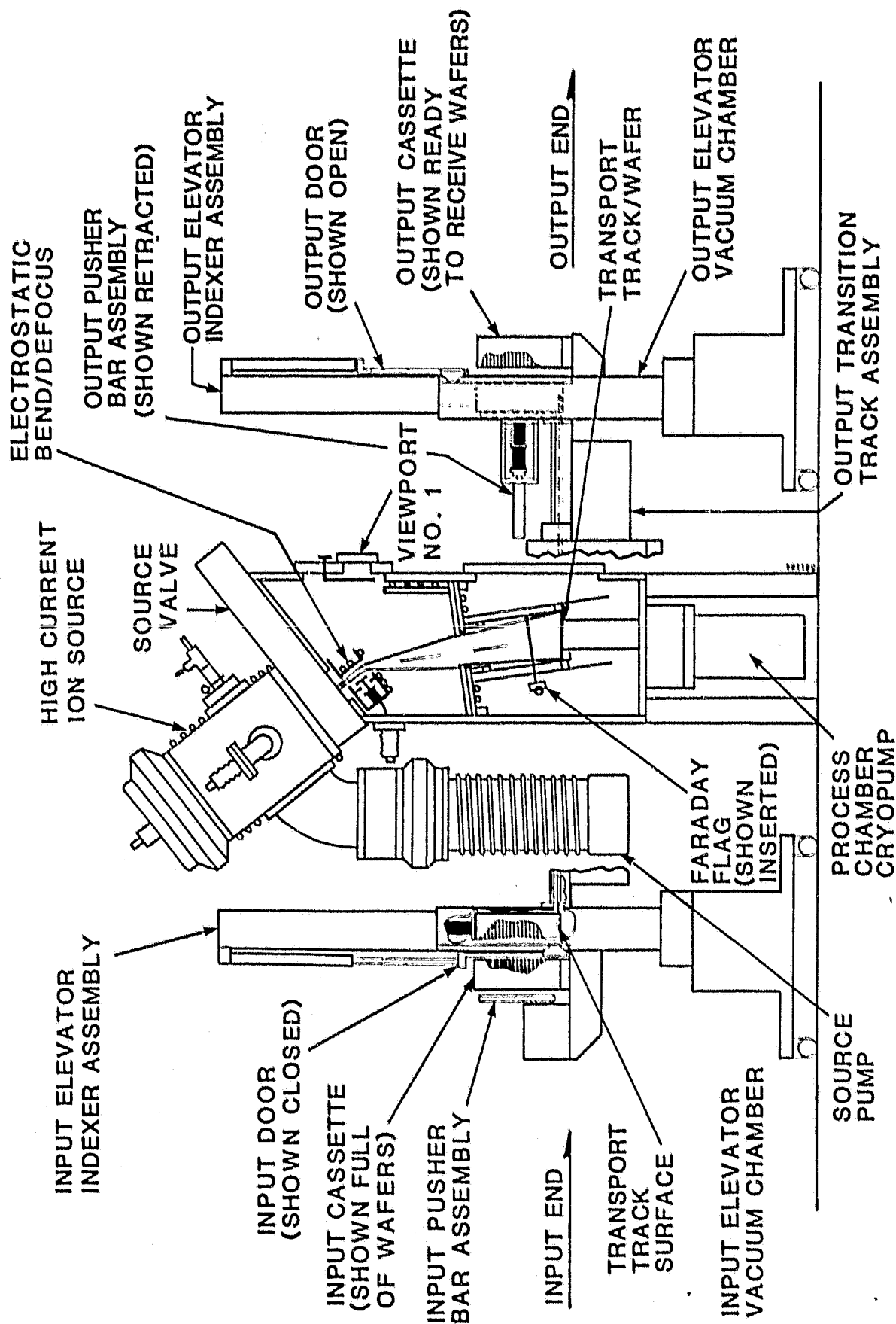


FIGURE 6. HIGH THROUGHPUT ION IMPLANTATION SYSTEM
(Central Section Rotated 90° for clarity)

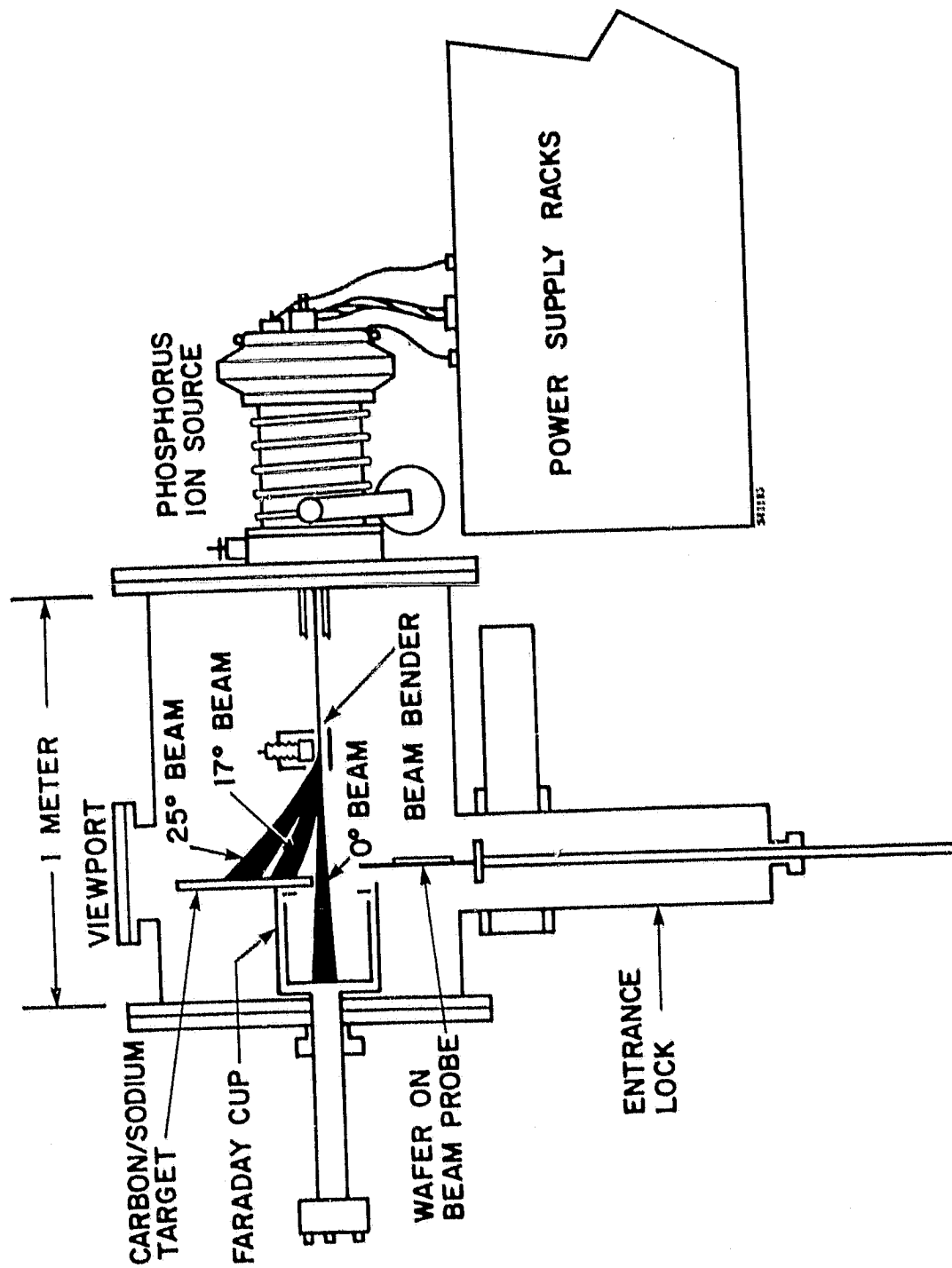


FIGURE 7. NMA TEST IMPLANT CHAMBER

The ion source is commercially available from Extrion. The extraction geometry was modified to permit operation at 10 keV with a well-focussed beam. Other beam energies are available and will be the subject of future experiments.

The beam bender was of a form shown in Figure 8. Plate separation was 1.5 inches. Although experiments have been performed on other shape electrodes, simple parallel plates have produced the best results to date. Voltages up to -12 kV have been used successfully.

The Faraday cup was a large area unit with electron suppression. The carbon target mounted on the cup was used to display the beam spot produced by the bend. The target was scored with a ruled pattern to permit measurements of the spot dimensions. Finally, the target was impregnated with sodium to allow a distinct orange glow to be created in zones where the beam struck.

The beam probe served two purposes. It could be used as an occulting mask to measure the dimensions of the unbent beam. It also served as the wafer carrier during the NMA implant, since it could conveniently be removed through an entrance lock without venting the system. Note that the probe could be rotated on axis to avoid normal incidence implants, if desired. However, for the 17° and 25° bent beams, far from normal incidence of implant was inevitable. Because of the fan in beam angles, a wide range of implant angles per wafer was produced.

Several tests to analyze the beam have been completed. The phosphorus beam was mass analyzed using a commercial ion implanter as a mass spectrometer. Figure 9 shows a log plot of the major species created. The main contaminant is oxygen since some of the phosphorus has a surface oxide growth. There are several species of phosphorus, since the normal gaseous form at moderate temperatures is P_4 . The heat of the ion source breaks up the P_4 molecule into lower forms, as can be seen in the figure.

The beam bender was tested to determine the degree to which simple theory failed to account for space charge polarization effects. Figure 10 shows that significant deviation begins to occur when the bender voltage is 50 percent of the ion beam voltage. These data correspond to the highest current, 6 milliamperes, available with the unmodified commercial ion source. A future experiment is designed to alter the source to increase the available current. This measurement, as well as others, will be remade at that time.

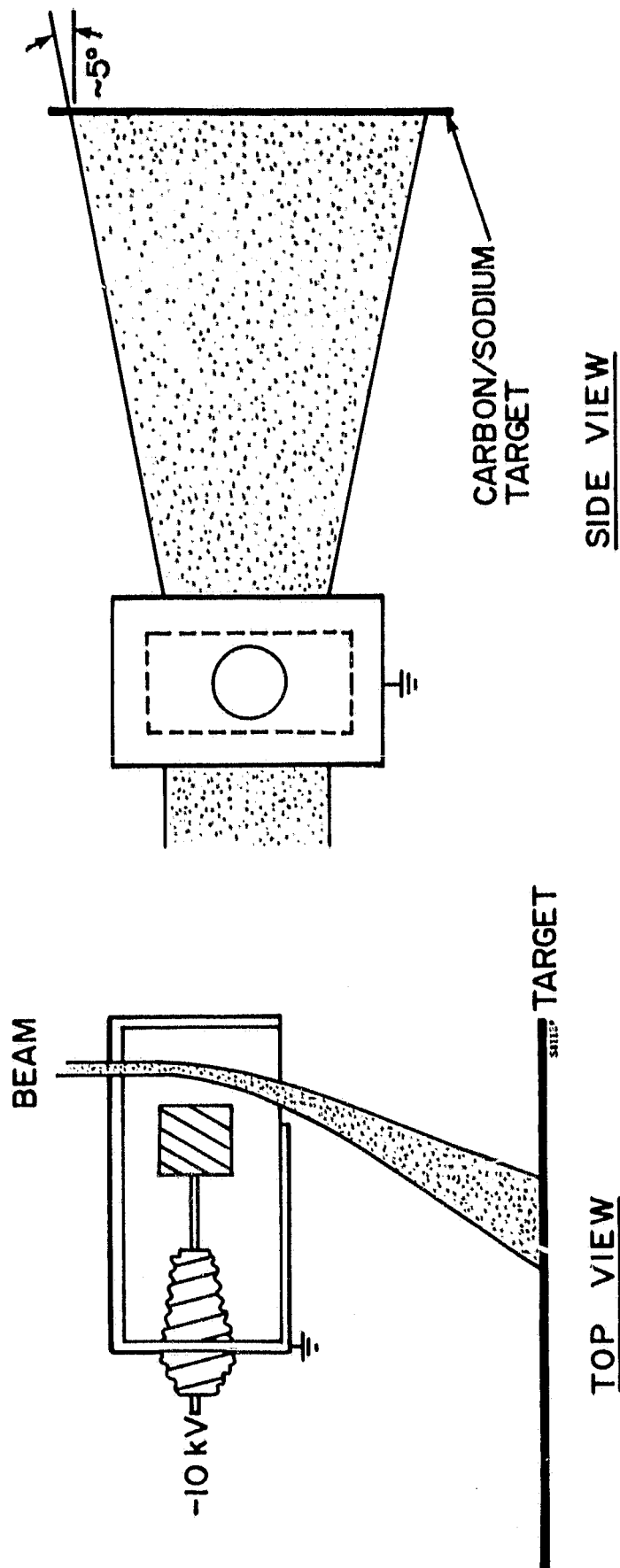


FIGURE 8. TEST MODEL BEAM BENDER

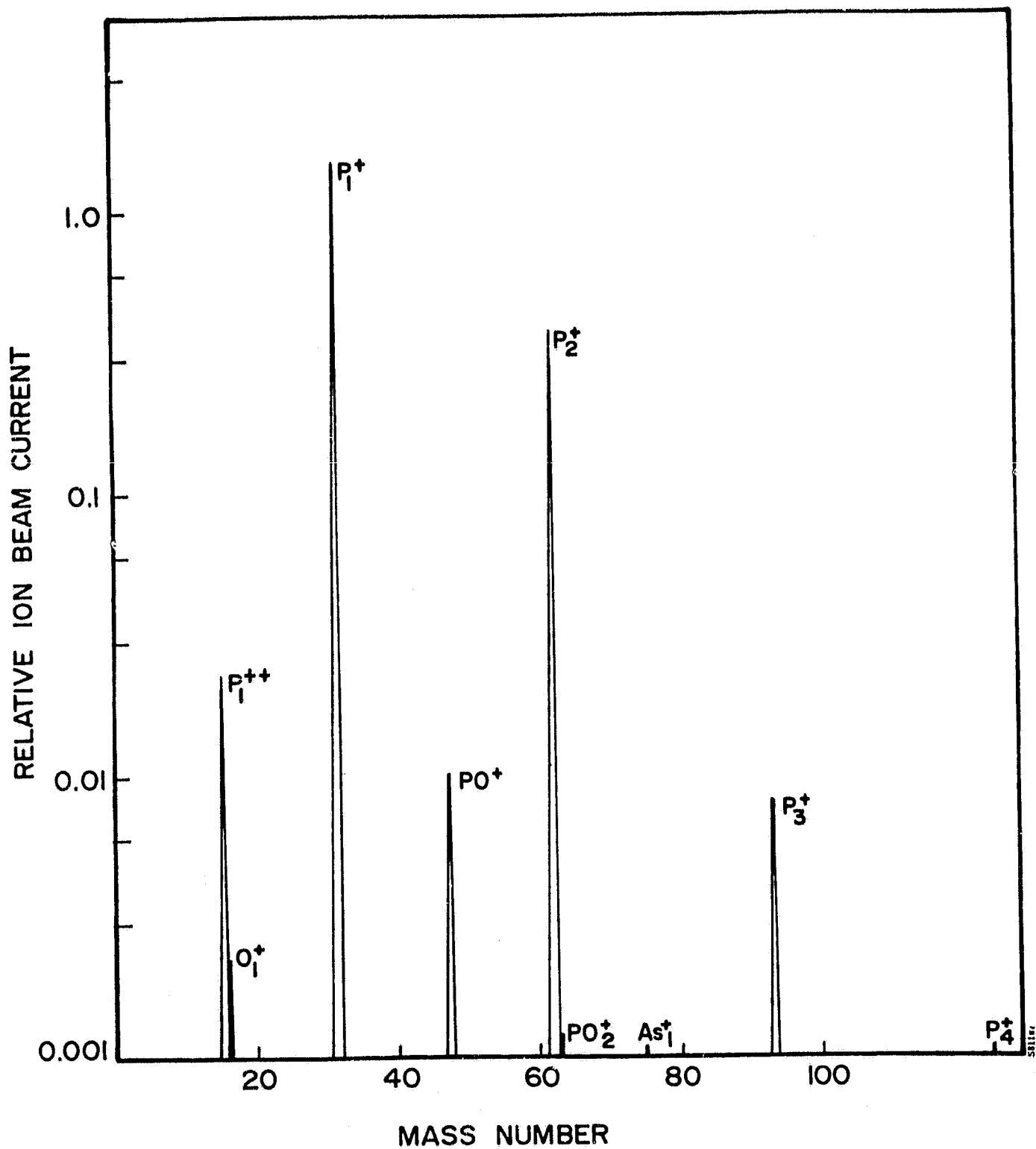


FIGURE 9. IONS PRODUCED BY COMMERCIAL GRADE SOLID PHOSPHORUS

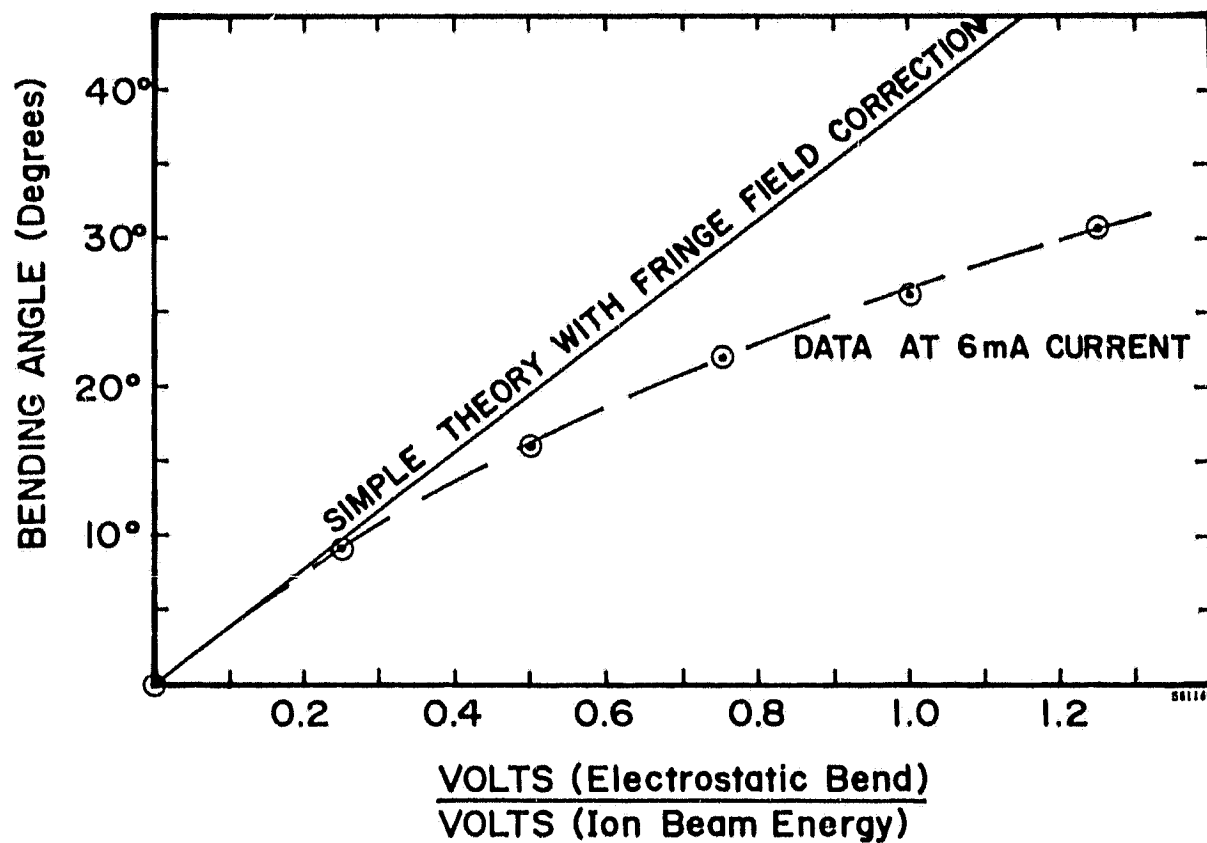


FIGURE 10. ELECTROSTATIC BEAM BENDING AT HIGH CURRENT

Figure 11 shows the horizontal (narrow beam axis) defocusing as a function of ion current. An initial rapid rise in divergence is observed as all of the neutralizing electrons are swept clear and the current is increased to the level where space charge becomes important. A second slope then appears at higher current, and this slope is relatively shallow. There is a suggestion that the slope is starting to increase at the present limiting beam current, and it will be important to repeat this measurement at high currents.

3.3.3 Solar Cell Data

The NMA test implants were made under rather difficult circumstances. The data to be presented is from nine wafers, the only ones actually implanted with this apparatus. There were three each at three bending angles plus three controls.

Implant dose depends on accurate knowledge of the area of the beam spot, as well as on data on the uniformity of the beam within the spot. Both of these quantities are known only poorly for the implanted wafers. In addition, some mechanical movement of the wafer on the probe was used to improve uniformity. However, this movement was human-powered, and the resulting uniformity is highly uncertain. It is known that at least a 1:2:4 dose variation exists between the three wafers at each bending angle, based on the time of the implant. It is estimated, however, that actual doses received vary between about 5×10^{14} to 1×10^{16} ions/cm² between all nine wafers.

Table 4 lists the cell performance. The table has been broken down into relative doses for the NMA implants and center/off-center for the controls. The controls have had this unusual separation because of the effect of the 30 keV neutral beam component in the Spire-operated JPL implanter. Even the off-center samples partially intercept the zone of the neutral beam spot, creating a slight decrease in average efficiency and V_{oc} . It should be noted that each entry is the average of six cells, except for the off-center controls, which average 12. The controls were implanted with a dose of 2.5×10^{15} ions/cm² and all implants were at 10 keV. All wafers had a boron-implanted BSF and all were co-processed except for the implant.

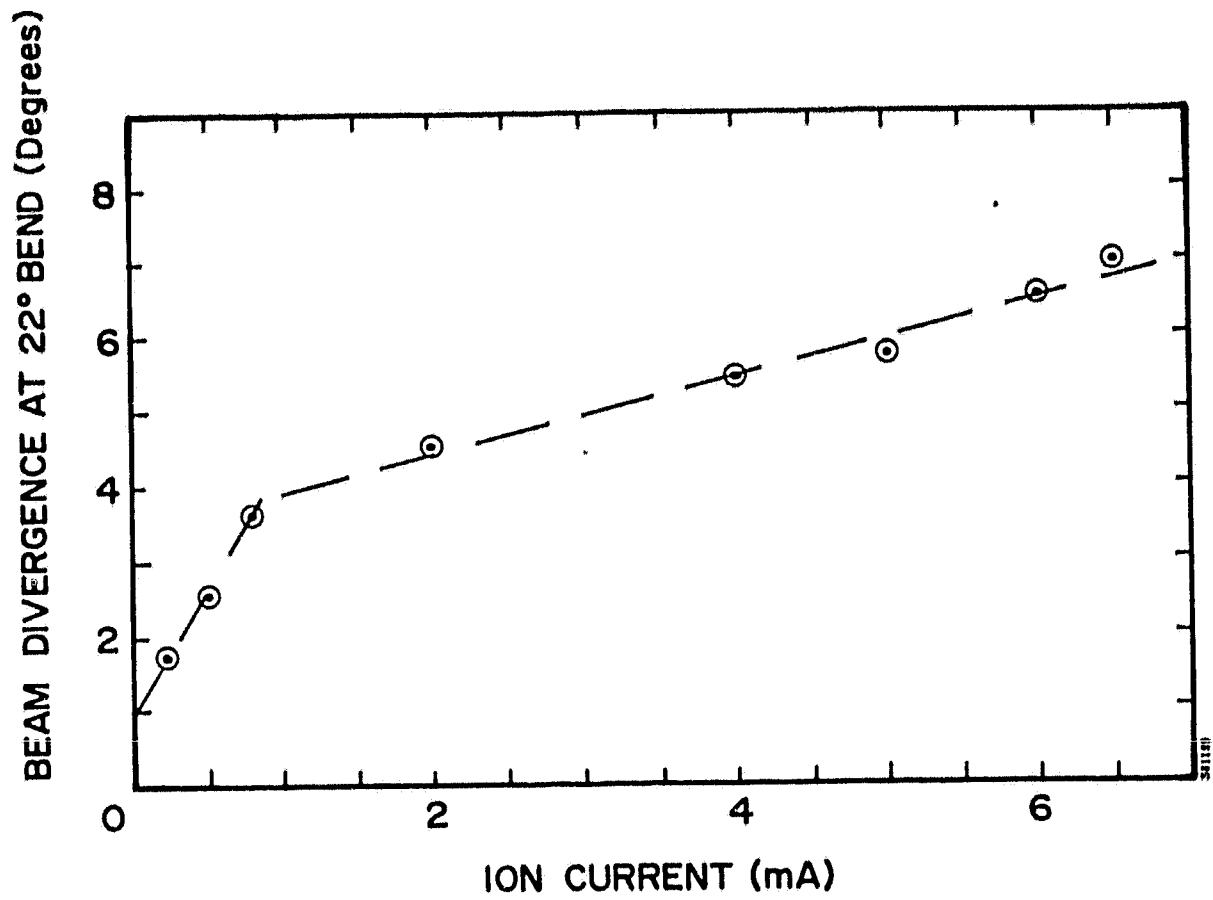


FIGURE 11. ION IMPLANTER BEAM SPREAD AFTER BEND/DEFOCUS

TABLE 4. NMA IMPLANTED CELL RESULTS

Wafer	V_{oc} (mV)	J_{sc} mA/cm ²	FF %	(AM0)* %	(AM1)** %
Control (center)	573 \pm 1	28.2 \pm 0.08	76.0 \pm 0.2	9.08 \pm 0.04	15.0 \pm 0.07
Control (off Center)	577 \pm 2	28.8 \pm 0.12	75.4 \pm 0.4	9.27 \pm 0.06	15.3 \pm 0.1
0° (dose=1)	580 \pm 1	28.8 \pm 0.21	74.8 \pm 0.9	9.22 \pm 0.9	15.2 \pm 0.1
0° (dose=2)	579 \pm 1	29.0 \pm 0.18	75.1 \pm 0.5	9.30 \pm 0.03	15.4 \pm 0.1
0° (dose=4)	579 \pm 2	28.8 \pm 0.27	75.3 \pm 0.8	9.26 \pm 0.10	15.3 \pm 0.2
17° (dose=2)	580 \pm 1	29.0 \pm 0.18	75.3 \pm 0.4	9.36 \pm 0.06	15.5 \pm 0.1
17° (dose=4)	579 \pm 1	28.7 \pm 0.18	75.7 \pm 0.4	9.29 \pm 0.04	15.3 \pm 0.1
25° (dose=1)	579 \pm 2	29.2 \pm 0.19	74.9 \pm 0.5	9.36 \pm 0.06	15.5 \pm 0.1
25° (dose=1)	579 \pm 1	29.0 \pm 0.19	75.5 \pm 0.5	9.35 \pm 0.03	15.4 \pm 0.1
25° (dose=4)	580 \pm 1	28.8 \pm 0.22	75.6 \pm 0.7	9.34 \pm 0.03	15.4 \pm 0.1

*No AR Coating

** Times 1.4 for AR coat and times 1.18 for AM1

The most obvious statement about these data is that there is very little difference between any of the cells, despite the wide variation in implant conditions. Only center controls differ by more than three standard deviations from the overall average, and this is explained by the neutral beam effect. There is no observable dose effect. The implants at 25° may have a marginally higher efficiency, especially compared to the 0° data. However, it is not obvious whether this subtle difference is due to bending away from neutral gas, a neutral beam effect, or the shallower implant. The latter is due to the steeper implant angle relative to the wafer surface. At 25° , this corresponds to an effective energy of 9.06 keV if the implants were at normal incidence. The possibility of improving the efficiency at lower implant energies will be explored in future testing.

Figure 12 compares the quantum efficiency of a typical NMA implant with a center control. It can be seen that there is a distinct loss only in the blue performance, consistent with the deep implant expected of a 30 keV neutral beam component. The very close match in quantum efficiency above 700 nanometers between these two widely differing implant techniques is indicating that a solid phosphorus source gives an NMA implant equivalent to mass analyzed techniques.

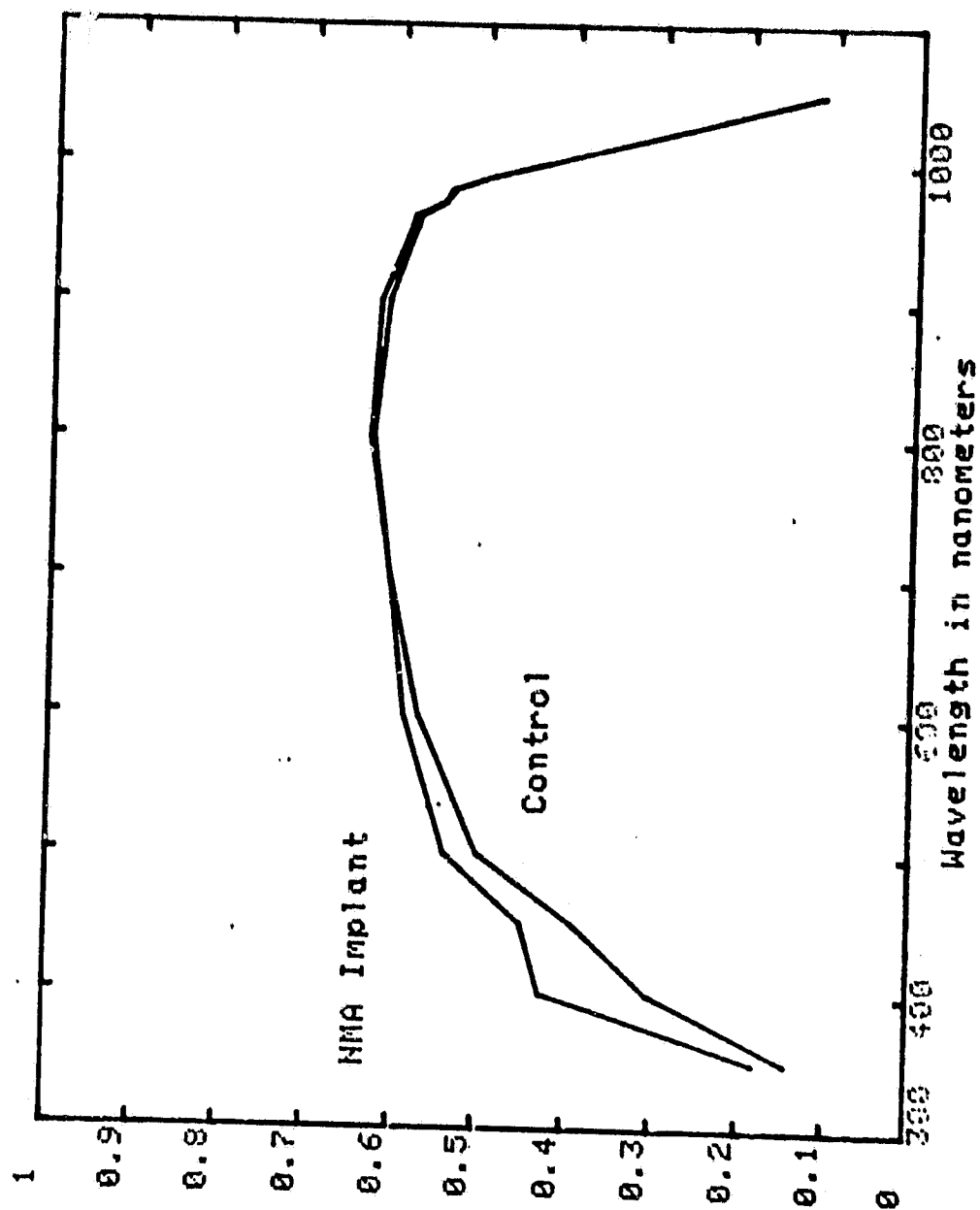


FIGURE 12. COMPARISON OF QUANTUM EFFICIENCY FOR
NMA IMPLANTS AND CENTER CONTROLS

SECTION 4

SCHEDULE AND FUTURE WORK

The pulser and transport are now complete with the exception of minor tuneups and rework to improve system performance and reliability. More work is needed to identify proper conditions for operation of the pulser and to insure reproducibility. The ion implanter task is only just beginning, and at least one further set of beam transport studies is required to provide a complete understanding before committing to the final design. In addition, the highly promising implant results have generated interest to pursue some further studies of implant parameters, particularly implant angle and energy. Figure 13 shows the current schedule for the implanter task pending the receipt of further funding.

FY 82

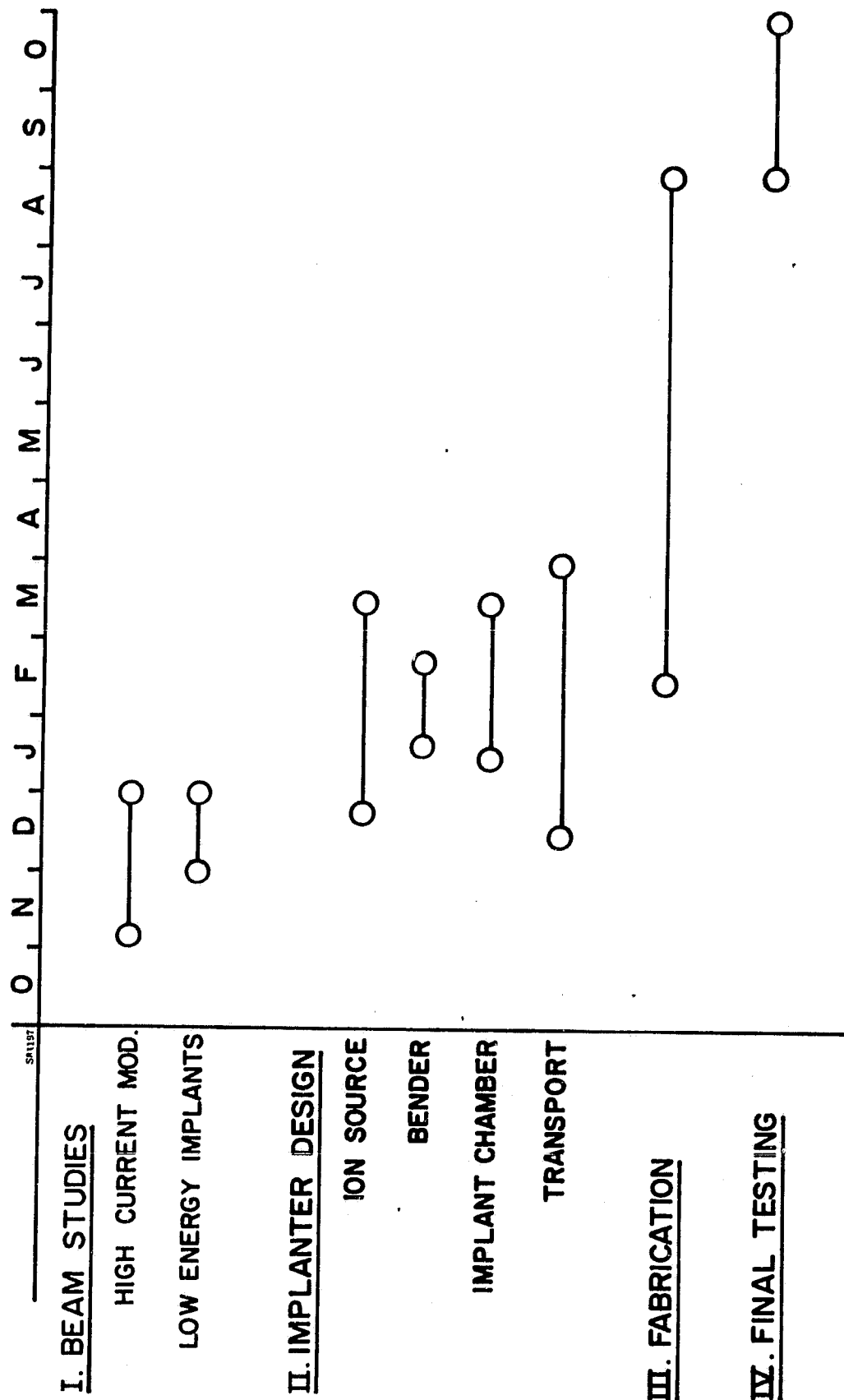


FIGURE 13. TASK 3 - NMA ION IMPLANTER FABRICATION